

## A method for prediction of unstable deformation in hot forging process by simulation

Shi-qiang LU<sup>1</sup>, Xin LI<sup>2</sup>, Ke-lu WANG<sup>2</sup>, Shi-biao LIU<sup>1</sup>, M. W. FU<sup>3</sup>

1. School of Materials Science and Engineering, Nanchang Hangkong University, Nanchang 330063, China;
2. School of Aeronautical Manufacturing Engineering, Nanchang Hangkong University, Nanchang 330063, China;
3. Department of Mechanical Engineering, The Hong Kong Polytechnic University, Kowloon, Hong Kong, China

Received 13 May 2013; accepted 29 September 2013

**Abstract:** A method is proposed for prediction of the unstable deformation in hot forging process using both the determined thermomechanical parameter windows of the unstable deformation zones and finite element simulation. Taking Ti–6.5Al–3.5Mo–1.5Zr–0.3Si alloy as the testing material, the thermomechanical parameter windows of the unstable deformation zones for the Ti-alloy are integrated into a commercial finite element simulation software platform. The distribution and variation of the unstable deformation zones of the alloy in hot compression process are simulated and predicted using the tailor-made finite element codes in the finite element platform. The simulation results tally with the physical experiments and the proposed method for simulation and prediction of the unstable deformation is thus verified and its efficiency is validated.

**Key words:** instability map; unstable deformation; instability deformation simulation; Ti–6.5Al–3.5Mo–1.5Zr–0.3Si; titanium alloy

### 1 Introduction

Forging is a prime working process for manufacturing of structural components with diverse applications. In aerospace industries, the requirements on microstructure and mechanical properties of the forged parts (forgings) have become more and more critical. To ensure the forgings with excellent microstructure and properties, the forged parts must be formed in the stable deformation zones in the processing map [1], not in the unstable deformation zones where unstable flow occurs. The well known metallurgical manifestations of flow instability are adiabatic shear band, flow localization, dynamic strain ageing, kink band, mechanical twinning and flow rotations [1,2]. The occurrence of unstable deformation, i.e. the flow instability described above, not only reduces the workability of metal, but also leads to the microstructure deterioration and property inhomogeneity, and further results in the deterioration of forging properties. Therefore, the hot forging in unstable deformation zones must be avoided.

Recently, the processing map technique developed

based on the dynamic materials model (DMM) provides an effective method for identification of the stable and/or unstable deformation conditions in metal hot working processes. In 1981, GEGEL [3] firstly proposed the theory of DMM and introduced a parameter called efficiency of power dissipation and a concept called power dissipation map. The efficiency of power dissipation is a dimensionless parameter which represents the relative rate of the internal entropy production during hot forging process and characterizes the dissipative microstructure at different temperatures and strain rates. The distribution of the efficiency of power dissipation with temperature and strain rate constitutes a power dissipation map.

Subsequently, PRASAD et al [4], GEGEL [5], MALAS et al [6] and ALEXANDER [7] further improved the theory of DMM and developed the processing map technique. By the thermodynamics and dissipative structure theory, the criteria for flow instability or stability used in the processing map technique are derived. Furthermore, using the criteria, the instability map is plotted and superimposed on the power dissipation map to form the processing map. From

the instability map or the processing map, the thermomechanical parameters (referring to the internal temperature, strain rate and strain in the deformed body) window for the stable and /or unstable deformation can be identified, which provides a basis to determine the external hot forging process parameters (referring to the heating temperature and deformation velocity applied to billet) to produce the forgings with the required microstructures and properties via avoiding the unstable deformation. The processing map technique has been used to control the microstructures and properties of the workpieces via the optimal design of hot working process parameters [8–13]. But the authors believe that such optimal hot working process parameters are the internal physical field variables, the so-called thermomechanical parameters in this work, in the deformed body. The thermomechanical parameters of inside the deformed body are not uniform. The optimal hot working process parameters identified by the processing map technique are thus difficult to be applied in practice as the external hot working (or forging) process parameters.

On the other hand, the finite element (FE) simulation technique provides an effective approach for evaluating and determining the distribution and variation of thermomechanical parameters in the deformed body in hot forging process. Despite the fact that hot forging process is complicated and affected by many factors including material properties, original material microstructure, hot forging process parameters, friction condition and die structure, etc, the FE simulation provides an efficient approach to revealing the deformation behavior in hot forging process in such a way to help the determination of external hot forging process parameters, die design, and forging quality control since LEE and KOBAYASHI [14] firstly proposed the Lagrange algorithm based rigid-plastic FE method in 1973. Presently, many FE simulation commercial software systems are available. Considering increment of temperature in forging system due to the conversion of plastic deformation work to thermal energy as well as this thermal-mechanical coupling effect, FE simulation is an effective approach to well simulating the instantaneous deformation and to predicting the forging shape. In addition, it can also determine the temperature, strain rate, stress, strain and velocity distribution in hot forging process and help to optimize the external hot forging process parameters, billet design and die structure [14–16]. Such a FE-based optimization has not yet been used in the optimal design of the external hot forging process parameters for the avoidance of unstable deformation.

Considering the fact that the identified thermomechanical parameter windows of the stable and/or unstable deformation zones based on the

processing map technique are difficult to be applied in practice as the external hot forging process parameters such as heating temperature and deformation velocity applied to billet, the processing map technique and the FE simulation are thus used simultaneously in this research, namely, the thermomechanical parameter windows of the unstable deformation zones determined by the instability map or the processing map are compared with the thermomechanical parameters identified by the FE simulation, the unstable deformation location inside the deformed body as well as its variation in hot forging process can thus be identified, and the external hot forging process parameters for the avoidance of the unstable deformation can also be optimized. Such the optimized external hot forging process parameters can be used to guide the practical forging production. It thus provides a basis for avoiding unstable deformation, improving material forging workability, and ensuring the formed parts with the desirable microstructures and properties.

In tandem with the above-described goals, a method for prediction of the unstable deformation in hot forging process with the thermomechanical parameter windows of the unstable deformation zones determined by instability map and FE simulation is proposed. The method can be used not only to predict the distribution and variation of the unstable deformation zones with the given external hot forging process parameters, but also to figure out the external hot forging process parameters under which the unstable deformation does not occur. Meanwhile, it is easy to be realized via tailor-made FE codes based on the commercial FE software. As a case study, the hot compressing of Ti–6.5Al–3.5Mo–1.5Zr–0.3Si alloy at a constant strain rate is studied by the proposed method to verify its efficiency and validity.

## 2 Method for prediction of unstable deformation in hot forging process

### 2.1 Instability map and thermomechanical parameter windows

For a given temperature and strain, the dynamic response of material to strain rate can be represented by the following constitutive equation:

$$\bar{\sigma} = K \dot{\varepsilon}^m \quad (1)$$

where  $\bar{\sigma}$  is the effective stress,  $\dot{\varepsilon}$  is the effective strain rate,  $K$  is a constant and  $m$  is the strain rate sensitivity defined as

$$m = \left[ \frac{\partial(\ln \bar{\sigma})}{\partial(\ln \dot{\varepsilon})} \right]_{\bar{\varepsilon}, T} \quad (2)$$

According to the theory of DMM [1,3], the power ( $P$ ) absorbed by workpiece from tooling in hot forging

process is dissipated as viscoplastic heat ( $G$ ) and microstructural change ( $J$ ), namely:

$$P = \bar{\sigma} \dot{\varepsilon} = G + J = \int_0^{\dot{\varepsilon}} \bar{\sigma} d\dot{\varepsilon} + \int_0^{\bar{\sigma}} \dot{\varepsilon} d\bar{\sigma} \quad (3)$$

On the basis of the extremum principle of the irreversible thermodynamics applied to the large plastic flow [1,5,17], the stable deformation, i.e. stable flow occurs when

$$\frac{\partial J}{\partial \dot{\varepsilon}} > \frac{J}{\dot{\varepsilon}} \quad (4)$$

Inversely, the unstable deformation, i.e. flow instability will happen if the differential quotient satisfies the following inequality:

$$\frac{\partial J}{\partial \dot{\varepsilon}} < \frac{J}{\dot{\varepsilon}} \quad (5)$$

Thus, a criterion for describing the occurrence of unstable deformation in hot forging process is developed and given by

$$\xi(\dot{\varepsilon}) = \frac{\partial \ln(\frac{m}{m+1})}{\partial \ln \dot{\varepsilon}} + m < 0 \quad (6)$$

The distribution of the instability parameter  $\xi(\dot{\varepsilon})$  meeting the inequality (6) in the frame of temperature and strain rate constitutes an instability map. According to the instability map, the thermomechanical parameter windows of the unstable deformation zones can thus be determined.

**2.2 FE simulation with built-in thermomechanical parameter windows**

After the instability maps are constructed based on the instability criterion inequality (6), and the thermomechanical parameter windows of unstable deformation zones are determined, the tailor-made FE codes on the top of a commercial FE software system are developed so that the thermomechanical parameter windows of the unstable deformation zones are built into the FE software system for simulation of the entire forming process. The detailed implementation process is as follows.

In FE simulation, upon the convergence of calculation at a specific deformation loading step, the comparison is made between the thermomechanical parameters (temperature, strain rate and strain) inside the deformed body and the thermomechanical parameter windows of the unstable deformation zones. If the thermomechanical parameters calculated by FE simulation at a specific tiny place inside the deformed body are within the thermomechanical parameter windows of the unstable deformation zones, the deformation in the specific tiny place is defined as the

unstable deformation. The specific tiny place is the unstable deformation zone and its range will be shown using nephogram in this work. Similarly, such a comparison is repeated at all other tiny places for each deformation loading step to reveal the unstable deformation zones so that the evolution of the unstable deformation zones in the entire forging process can be predicted and determined. By this approach, the unstable deformation under a given external hot forging process parameters can be predicted and the optimal external hot forging process parameters can be determined for avoiding the occurrence of the unstable deformation. Figure 1 shows a flow chart for simulation and prediction of the unstable deformation in hot forging process by FE simulation with the built-in thermomechanical parameter windows of the unstable deformation zones.

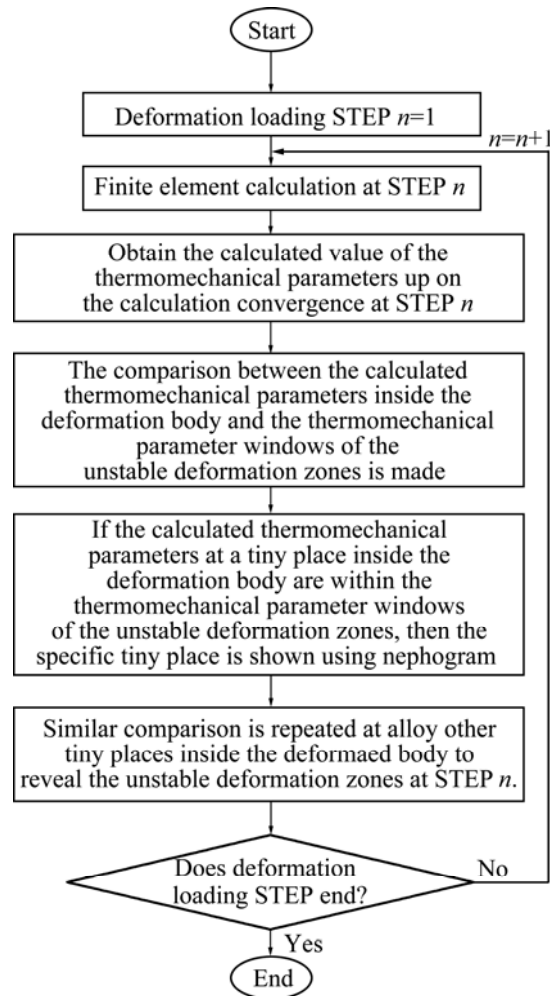


**Fig. 1** Flow chart for prediction of unstable deformation by FE simulation with built-in thermomechanical parameter windows of unstable deformation zones

The proposed method will not only overcome the disadvantage that the thermomechanical parameter windows of the unstable deformation zones predicted by instability map cannot be directly used in practice, but

also avoid the deficiency that the FE technique cannot simulate and predict the unstable deformation. The method is thus pragmatic and effective.

### 3 Prediction of unstable deformation in hot compressing process of Ti–6.5Al–3.5Mo–1.5Zr–0.3Si alloy

To verify the feasibility and validity of the proposed method, the simulation and prediction of the unstable deformation in hot compressing of Ti–6.5Al–3.5Mo–1.5Zr–0.3Si alloy was conducted as a case study.

#### 3.1 Thermomechanical parameter windows of unstable deformation zones

The as-received Ti–6.5Al–3.5Mo–1.5Zr–0.3Si alloy underwent the pre-forging sequentially at low, high and low temperatures and cooled down to room temperature in the air. Its microstructure is equiaxed  $\alpha$  and intergranular  $\beta$  grains, as shown in Fig. 2.

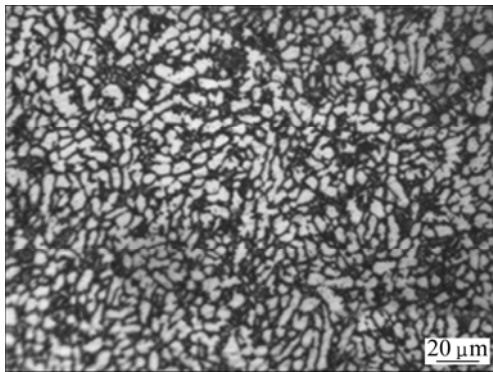


Fig. 2 Microstructure of as-received Ti–6.5Al–3.5Mo–1.5Zr–0.3Si alloy

To simulate and predict the unstable deformation of the Ti alloy in hot forging process, the thermomechanical parameter windows of the unstable deformation zones must be first determined based on its instability maps. The details are articulated in the following sections.

##### 3.1.1 Compression experiment

To construct the instability maps of the Ti alloy, the flow stresses of the Ti alloy at different temperatures, strain rates and strains are obtained using compression test. The compression tests under a constant strain rate were conducted in the temperature range of 780–990 °C with the interval of 30 °C and the strain rate range of 0.001–10 s<sup>-1</sup> with four testing points of 0.001, 0.01, 0.1 and 10 s<sup>-1</sup>. The dimensions of the sample were  $\phi 8$  mm $\times$ 12 mm. The compression was done in a THERMECMASTOR-Z hot working simulator. The maximum initial height reduction was 70%, which is equivalent to the effective strain of 1.2. The compression specimens were heated at a heating rate of 10 °C/s,

soaked at the testing temperature for about 150 s and cooled down immediately by helium gas-jet at a cooling rate of 45 °C/s after compression.

To observe the deformed microstructures, the compressed specimens were sectioned parallel to the compression axis and the cut surfaces were polished and etched with a solution of 1 mL HF + 3 mL HNO<sub>3</sub> + 5 mL H<sub>2</sub>O. The microstructure observation was done in an XJP–6A metallographic microscope.

##### 3.1.2 Instability maps

Based on the unstable deformation criterion designated by the inequality (6) and the flow stresses obtained at different temperatures, strain rates and strains in compression tests, the instability maps of the Ti alloy at different strains are constructed and shown in Fig. 3. It can be seen from Fig. 3 that the range of the unstable deformation zone has an appreciable expanding trend with strain. Considering the inhomogeneity of strain distribution inside the deformed body and in order to ignore the effect of strain on the unstable deformation zone, the assembly of the unstable deformation zones at different strains forms the unstable deformation zone of the whole deformation process, as shown in Fig. 4. The assembled unstable deformation zone is a little larger than the actual situation, which is thus safer to optimize the external hot forging process parameters for the avoidance of unstable deformation. From Fig. 4, the thermomechanical parameter windows of the unstable deformation zone are thus identified as 780–850 °C and 0.005–10 s<sup>-1</sup>, 850–940 °C and 0.01–10 s<sup>-1</sup>, 940–990 °C and 0.05–10 s<sup>-1</sup>, which will be used in the subsequent FE simulation.

#### 3.2 Simulation and prediction of unstable deformation in hot compression process

Upon the development of the tailor-made FE simulation codes on the commercial FE software DEFORM 3D by building-in the thermomechanical parameter windows of the unstable deformation zone using the approach presented in section 2.2, the unstable deformation in hot compression of the Ti alloy is then simulated and predicted using DEFORM 3D with the tailor-made codes.

##### 3.2.1 Simulation conditions

The hot compression was conducted at a constant strain rate. The heating temperature was 900 °C, and the strain rates were 1.0, 0.01 and 0.001 s<sup>-1</sup>, which fall into the unstable deformation zone, near the boundary of the unstable deformation zone and the stable deformation zone respectively, as shown in Fig. 4. In the compression process, the temperatures of upper and lower punches are 800 °C and the room temperature is 25 °C. The shear friction factor is 0.2, and the heat transfer coefficient between the specimen and punch is 1000 W/(m<sup>2</sup>·K), and

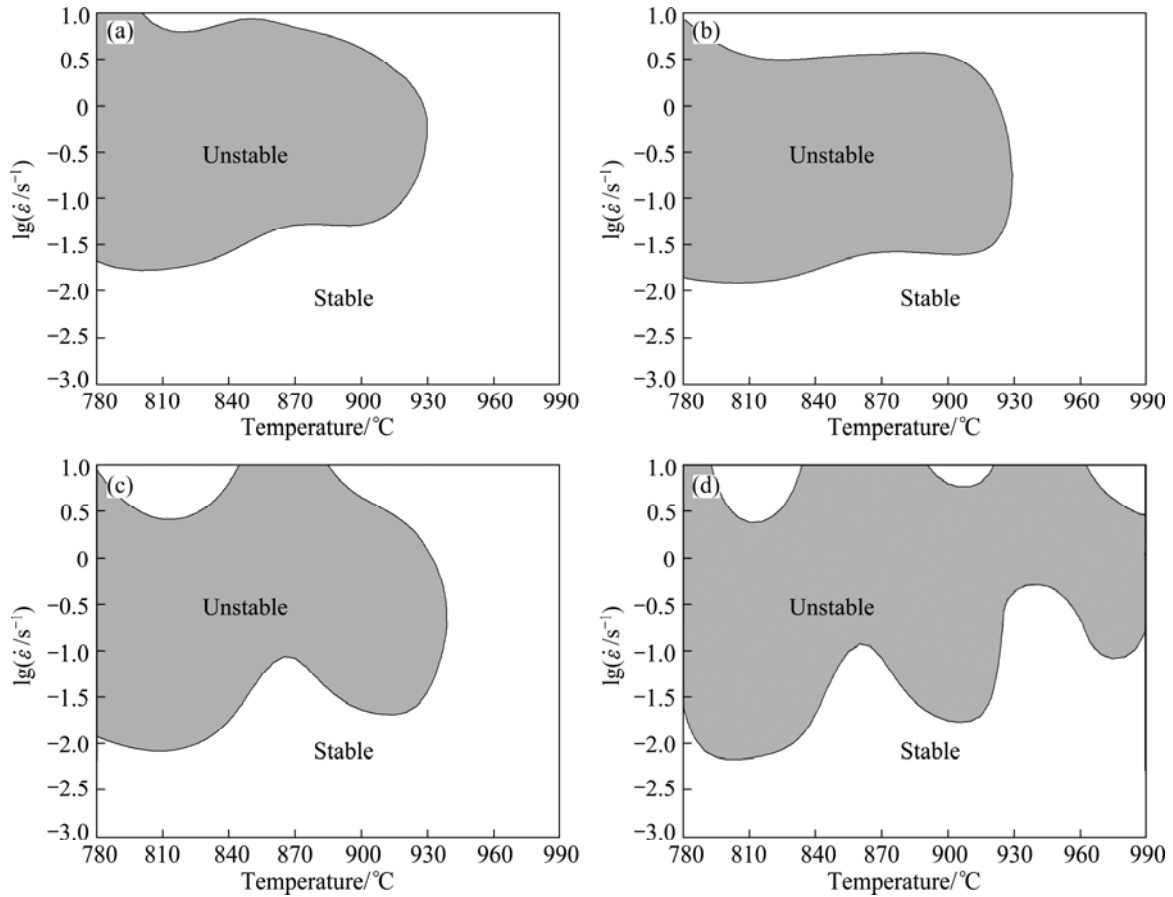


Fig. 3 Instability maps of Ti alloy at different strains: (a)  $\varepsilon=0.2$ ; (b)  $\varepsilon=0.5$ ; (c)  $\varepsilon=0.8$ ; (d)  $\varepsilon=1.1$

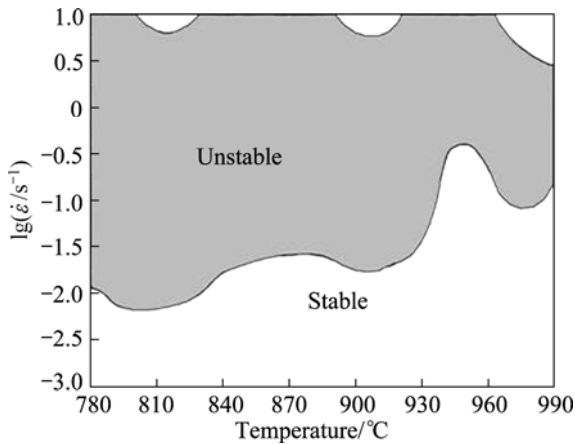


Fig. 4 Instability map obtained by superposing unstable zones at different strains

the convection coefficient between the specimen and air is  $20 \text{ W}/(\text{m}^2\cdot\text{K})$ .

3.2.2 Results and discussion

The simulation results of the unstable deformation in compression of the Ti alloy at  $900 \text{ }^\circ\text{C}$  and the strain rates of  $1.0, 0.01$  and  $0.001 \text{ s}^{-1}$  are shown in Figs. 5(a), (b) and (c), respectively. In Fig. 5, the red color represents the unstable deformation zone and the blue color designates the stable deformation zone. The upper

numbers are the height reduction of the specimens.  $p_1, p_2, p_3$  and  $p_4$  are the identified points for the analysis of plastic deformation mechanisms at the different zones in the specimen.

From Fig. 5, it can be seen that when the specimen is compressed at  $900 \text{ }^\circ\text{C}$  and  $1.0 \text{ s}^{-1}$ , the specimen entirely falls into the unstable deformation zone. When the specimen is compressed at  $900 \text{ }^\circ\text{C}$  and  $0.01 \text{ s}^{-1}$ , the unstable deformation firstly occurs at the central of the specimen and the external circle of the upper and bottom surfaces of the specimen, and then extends to the whole specimen upon the completion of compression. When the specimen is compressed at  $900 \text{ }^\circ\text{C}$  and  $0.001 \text{ s}^{-1}$ , the specimen entirely falls into the stable deformation zone in the hot compression process.

The changes of temperature and strain rate for the four labeled points in Fig. 5 with the compression are shown in Figs. 6 and 7, respectively. From Fig. 6(a) and Fig. 7(a), it can be seen that when the sample is compressed at  $900 \text{ }^\circ\text{C}$  and  $1.0 \text{ s}^{-1}$ , the temperature of points  $p_1-p_4$  increases with the height reduction due to the higher strain rate. There is a larger temperature difference among these points. This indicates that the unstable deformation mechanisms such as adiabatic shear band and flow localization may occur in the hot

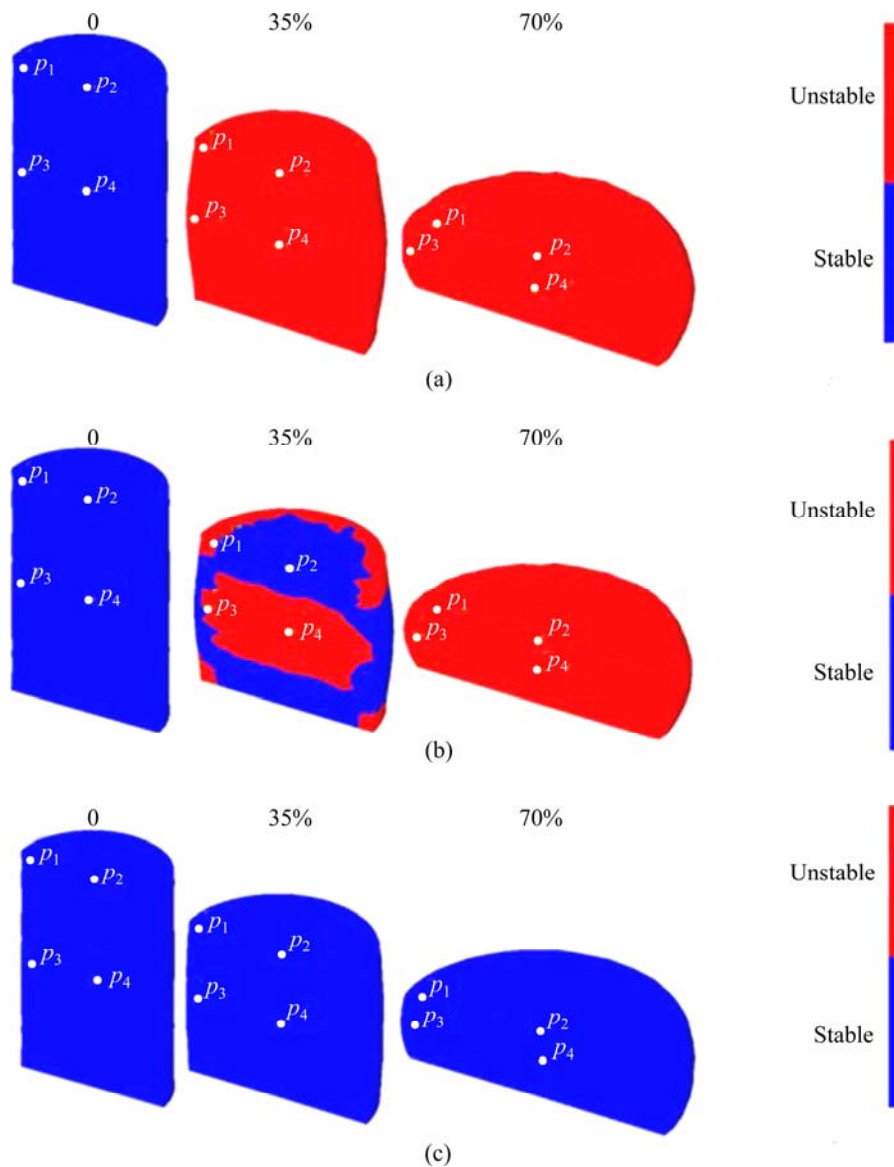


**Fig. 5** Simulation of unstable deformation in compression of Ti alloy at 900 °C and different strain rates: (a) 1.0 s<sup>-1</sup>; (b) 0.01 s<sup>-1</sup>; (c) 0.001 s<sup>-1</sup>

deformation process. Since point  $p_4$  is in the large deformation zone and point  $p_2$  is located at the difficult deformation zones, the temperature of point  $p_4$  increases most quickly and the temperature of point  $p_2$  increases most slowly. The strain rates of points  $p_1$  and  $p_4$  firstly increase and then decrease with increasing height reduction, but the strain rate of point  $p_2$  firstly decreases and then increases with increasing height reduction. The strain rate of point  $p_3$  continuously decreases with increasing height reduction. The strain rate variation of the points discussed above reflects that the strain rate difference among the zones where the points are located is large and the homogeneity and the coordination of deformation are not very good, which makes the unstable deformation occur easily. These changing characteristics of temperature and strain rate of points  $p_1$ – $p_4$  further

indicate that the results of simulation and prediction as shown in Fig. 5(a) are correct, which reveals that the specimen entirely falls into the unstable deformation zones in the deformation condition of 900 °C and 1.0 s<sup>-1</sup>.

In Fig. 6(b) and Fig. 7(b), when the specimen is compressed at 900 °C and 0.01 s<sup>-1</sup>, the temperature of points  $p_1$ – $p_4$  decreases with increasing height reduction. The reason is that the heat transferred from the specimen to environment is much more in the deformation at lower strain rate. Furthermore, the temperature difference among these points is smaller and will disappear with increasing compression. The strain rates of points  $p_1$  and  $p_4$  firstly increase and then decrease with increasing height reduction. The strain rate of point  $p_2$  is the lowest. Furthermore, it firstly decreases and then increases with the compression. The strain rate of point  $p_3$  continuously

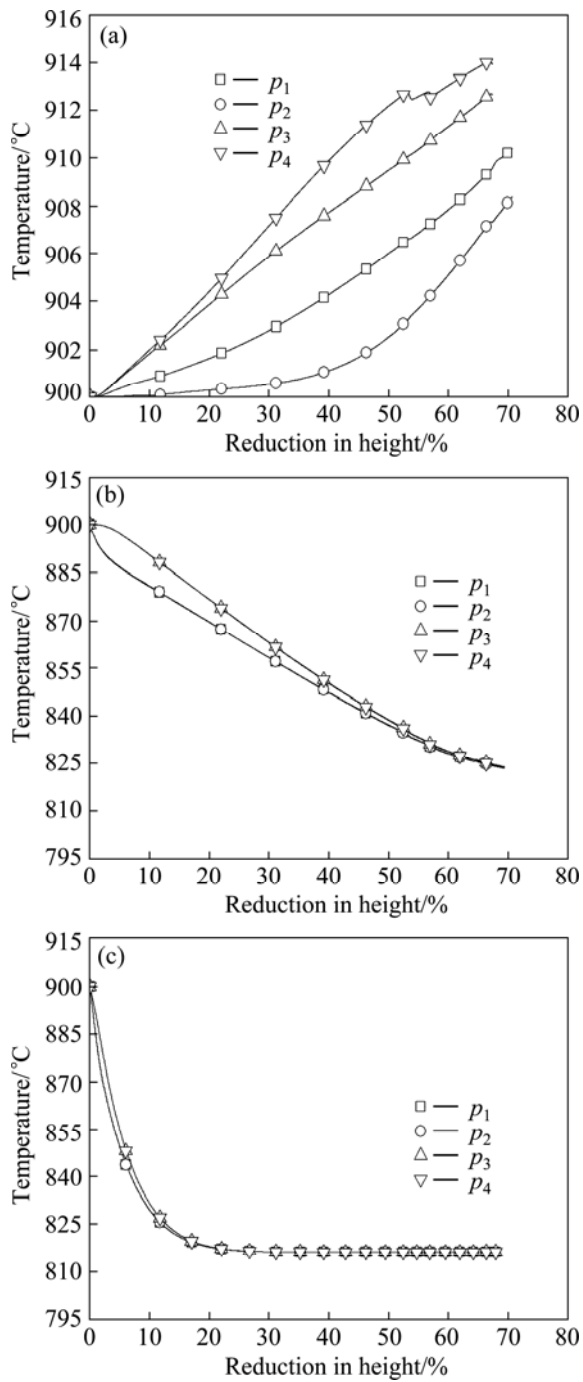


**Fig. 6** Temperature variation of labeled points in specimen compressed at 900 °C and different strain rates: (a)  $1.0 \text{ s}^{-1}$ ; (b)  $0.01 \text{ s}^{-1}$ ; (c)  $0.001 \text{ s}^{-1}$

decreases in the deformation process. Compared with the specimen compressed at 900 °C and  $1.0 \text{ s}^{-1}$ , the distribution homogeneity of temperature and strain rate of the specimen compressed at 900 °C and  $0.01 \text{ s}^{-1}$  is improved a little bit and thus the homogeneity and the coordination of deformation are improved too. From Fig. 7(b), before the height reduction of 35%, the strain rates at points  $p_1$ ,  $p_3$  and  $p_4$  are much higher than that of point  $p_2$  and thus the unstable deformation first occurs in the central of the specimen and the external circle of the

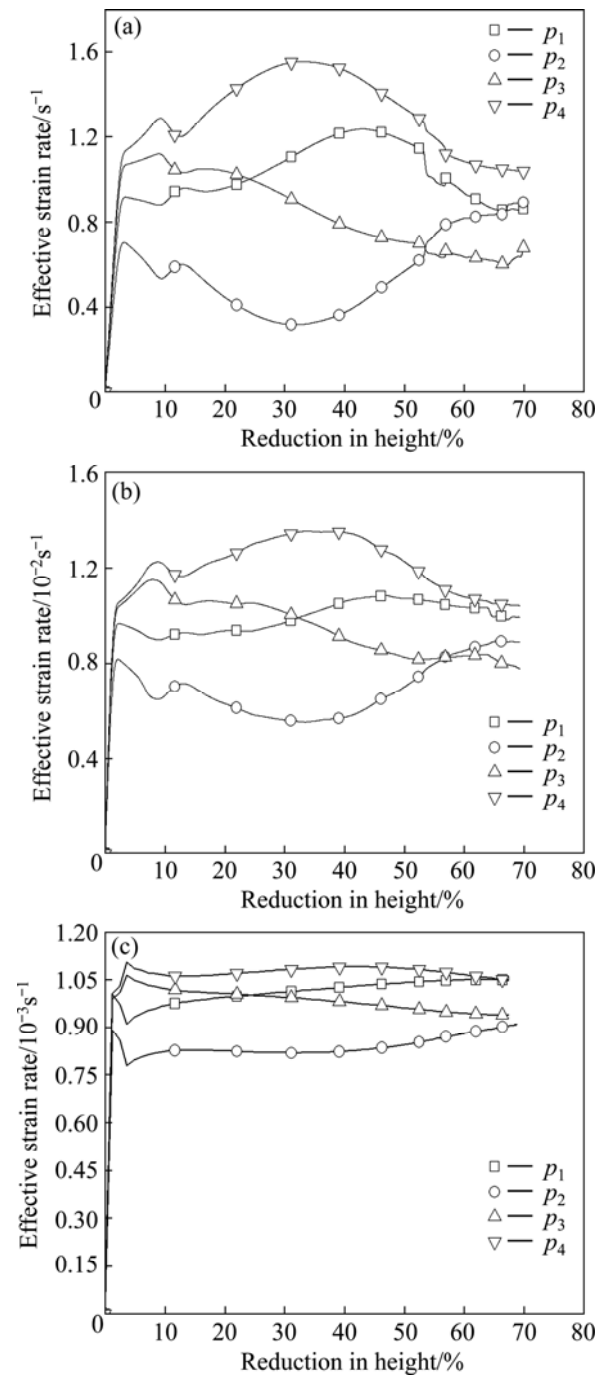


**Fig. 7** Strain rate variation of labeled points in specimens compressed at 900 °C and different strain rates: (a)  $1.0 \text{ s}^{-1}$ ; (b)  $0.01 \text{ s}^{-1}$ ; (c)  $0.001 \text{ s}^{-1}$

upper and bottom surfaces of the specimens. With the height reduction more than 35%, the strain rate of point  $p_2$  obviously increases and the unstable deformation thus extends to the entire specimen, as shown in Fig. 5(b).

Figure 6(c) and Fig. 7(c) show that when the specimen is compressed at 900 °C and  $0.001 \text{ s}^{-1}$ , the temperature difference among points  $p_1$ – $p_4$  is very small and the temperatures of these points decrease quickly at first, and then slowly to a stable constant, and eventually equal to the temperature of punch. This is because the

heat transferred from the specimen to the external is much more at a much lower strain rate. Compared with the scenarios of the specimens compressed at 900 °C and 0.1 s<sup>-1</sup> and 900 °C and 0.01 s<sup>-1</sup>, the strain rate difference among these points in the specimen compressed at 900 °C and 0.001 s<sup>-1</sup> is much smaller and the variation of strain rate in each point is not much. The relatively homogeneous distribution of the temperature and strain rate in the specimen compressed at 900 °C and 0.001 s<sup>-1</sup> shows that the deformation in the specimen is relatively homogeneous and always stable, which also tallies with the simulation results shown in Fig. 5(c).

#### 4 Microstructure observation and verification

To verify the simulation results of the unstable deformation, optical microscopy observation was carried out on the specimens compressed at 900 °C and different strain rates of 1.0, 0.01 and 0.001 s<sup>-1</sup>. The results are shown in Fig. 8, where the bright is  $\alpha$  phase and the dark is  $\beta$  phase.

From Fig. 8, it can be seen that the flow localization occurs where  $\alpha$  phase is long strip along the flow direction under the external compressing process parameters of 900 °C and 1.0 s<sup>-1</sup>, 900 °C and 0.01 s<sup>-1</sup>. This suggests that flow localization, which is the unstable deformation, occurs in these two process parameter configurations. In the external process

parameter configuration of 900 °C and 0.001 s<sup>-1</sup>,  $\alpha$  and  $\beta$  phases distribute homogeneously and the phase boundary between  $\alpha$  and  $\beta$  is blurry (see Fig. 8(c)). Furthermore, the unstable deformations such as adiabatic shear band and flow localization have not yet been observed (see Figs. 8(c) and (d)). Using tensile test, LI et al [18] found out that this material shows superplasticity with the elongation of 595% in the external tensile process parameters of 900 °C and 0.001 s<sup>-1</sup>, which suggests that superplastic deformation happens in this process parameter configuration. It is well known that superplastic deformation is a stable deformation. The above results obtained via metallographic observation are consistent with those of the simulation and the prediction of the unstable deformation shown in Fig. 5.

#### 5 Conclusions

1) A method to predict the unstable deformation in hot forging process is proposed using FE simulation with the built-in thermomechanical parameter windows of the unstable deformation zones determined by instability map. This method is simple and easy to implement.

2) Using the proposed method, the distribution and variation of the unstable deformation zones in compression of Ti-6.5Al-3.5Mo-1.5Zr-0.3Si alloy is simulated at the temperature of 900 °C and the strain rates of 1.0, 0.01 and 0.001 s<sup>-1</sup>. The results of FE simulation have a good agreement with experiments,

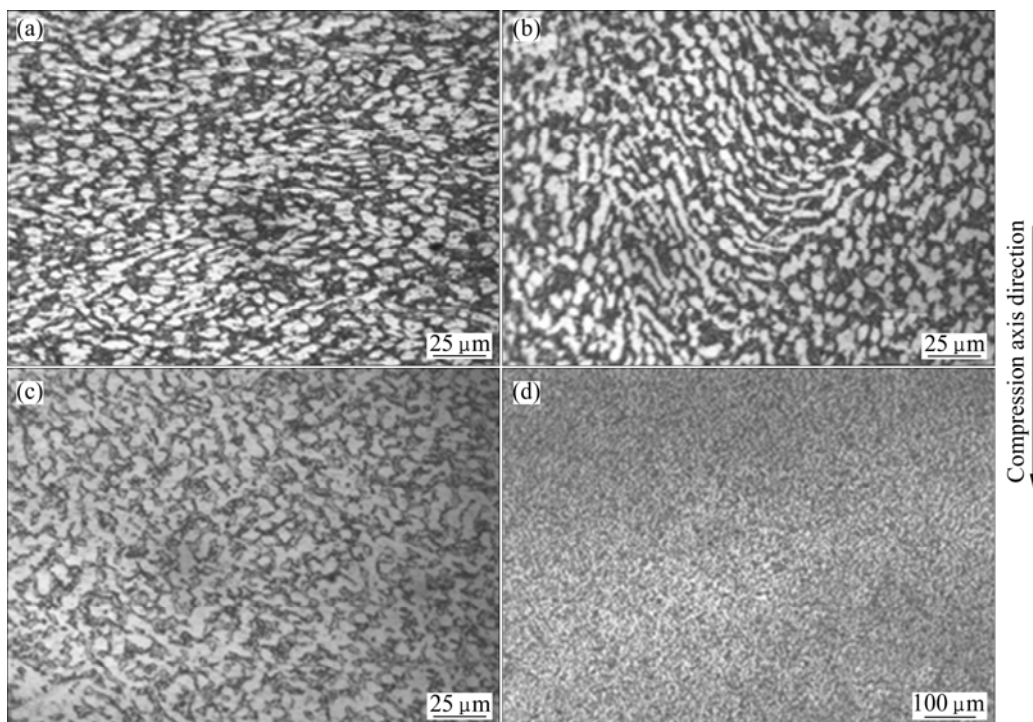


**Fig. 8** Microstructures at central zone of specimens compressed 70% in height reduction at 900 °C and different strain rates: (a) 1.0 s<sup>-1</sup>; (b) 0.01 s<sup>-1</sup>; (c), (d) 0.001 s<sup>-1</sup>

which verifies the validity of the proposed method.

3) The proposed method can predict the distribution and variation of the unstable deformation zones under a given external hot forging process parameter configuration, and can also determine and optimize the external hot forging process parameters in which the unstable deformation does not occur.

4) The optimized external hot forging process parameters can be used to guide the practical forging production in such a way to avoid forging defects and produce the forgings with the required microstructures and properties.

## References

- [1] PRASAD Y V R K, SASIDHARA S. Hot working guide: A compendium of processing maps [M]. OH: ASM International, The Materials Information Society, 1997.
- [2] LU Shi-qiang, LI Xin, WANG Ke-lu, DONG Xian-juan, LI Zhen-xi, CAO Chun-xiao. Dynamic material model theory and its application for controlling microstructures and properties of hot worked materials [J]. Chinese Journal of Mechanical Engineering, 2007, 43(8): 77–85. (in Chinese)
- [3] GEGEL H L. Material behavior modeling—An overview [M]. OH: ASM, 1983.
- [4] PRASAD Y V R K, GEGEL H L, DORAIVELU S M, MALAS J C, MORGAN J T, LARK K A, BARKER D R. Modeling of dynamic material behavior in hot deformation: Forging of Ti-6242 [J]. Metallurgical Transactions A, 1984, 15(10): 1883–1892.
- [5] GEGEL H L. Synthesis of atomistics and continuum modeling to describe microstructure, computer simulation in materials science [M]. OH: ASM, 1986.
- [6] MALAS J C, SEETHARAMAN V. Using material behavior models to develop process control strategies [J]. Journal of the Minerals, Metals and Materials Society, 1992, 6: 8–14.
- [7] ALEXANDER J M. Modelling of hot deformation of steels [M]. Berlin: Springer Verlag, 1989.
- [8] LU Shi-qiang, LI Xin, WANG Ke-lu, DONG Xian-juan, FU M W. High temperature deformation behavior and optimization of hot compression process parameters in TC11 titanium alloy with coarse lamellar original microstructure [J]. Transactions of Nonferrous Metals Society of China, 2013, 23: 353–360.
- [9] LI Xin, LU Shi-qiang, FU M W, WANG Ke-lu, CAO Chun-xiao. Analysis and comparison of the instability regimes in the processing maps generated using different instability criteria for Ti–6.5Al–3.5Mo–1.5Zr–0.3Si alloy [J]. Materials Science and Engineering A, 2013, 576: 259–266.
- [10] LI Hui-zhong, ZENG Min, LIANG Xiao-peng, LI Zhou, LIU Yong. Flow behavior and processing map of PM Ti–47Al–2Cr–0.2Mo alloy [J]. Transactions of Nonferrous Metals Society of China, 2012, 22: 754–760.
- [11] LUO J, LI M Q, YU W X, LI H. Effect of the strain on processing maps of titanium alloys in isothermal compression [J]. Materials Science and Engineering A, 2009, 504: 90–98.
- [12] SUN Y, ZENG W D, ZHAO Y Q, ZHANG X M, MA X, HAN Y F. Constructing processing map of Ti40 alloy using artificial neural network [J]. Transactions of Nonferrous Metals Society of China, 2011, 21: 159–165.
- [13] WANG K L, LU S Q, FU M W, LI X, DONG X J. Identification of the optimal ( $\alpha+\beta$ ) forging process parameters of Ti–6.5Al–3.5Mo–1.5Zr–0.3Si based on processing-maps [J]. Materials Science and Engineering A, 2010, 527: 7279–7285.
- [14] LEE C H, KOBAYASHI S. New solutions to rigid-plastic deformation problems using a matrix method [J]. Journal of Engineering for Industry, 1973, 3: 865–873.
- [15] HE Zhao, WANG He-nan, WANG Meng-jun, LI Guang-yao. Simulation of extrusion process of complicated aluminium profile and die trial [J]. Transactions of Nonferrous Metals Society of China, 2012, 22: 1732–1737.
- [16] ZHANG W, LIU Y, WANG L, LIU B. Numerical simulation and physical analysis for dynamic behaviors of P/M TiAl alloy in hot-packed forging process [J]. Transactions of Nonferrous Metals Society of China, 2012, 22: 901–906.
- [17] PRASAD Y V R K. Author's reply: Dynamic materials model, basis and principles [J]. Metallurgical and Materials Transactions A, 1996, 27: 235–236.
- [18] LI Xin, LU Shi-qiang, WANG Ke-lu, DING Lin-hai. Superplastic deformation behavior of TC11 titanium alloy at 900 °C [J]. Materials for Mechanical Engineering, 2009, 33(2): 21–24. (in Chinese)

# 一种预测金属锻造过程失稳变形的模拟方法

鲁世强<sup>1</sup>, 李鑫<sup>2</sup>, 王克鲁<sup>2</sup>, 刘诗彪<sup>1</sup>, 傅铭旺<sup>3</sup>

1. 南昌航空大学 材料科学与工程学院, 南昌 330063 ;
2. 南昌航空大学 航空制造工程学院, 南昌 330063 ;
3. 香港理工大学 机械工程系, 香港九龙

**摘要:** 提出一种利用失稳变形区热力参数窗口条件和有限元模拟相结合来预测锻造失稳变形的模拟方法, 并以 Ti–6.5Al–3.5Mo–1.5Zr–0.3Si 合金为例, 将该钛合金的失稳变形区热力参数窗口条件集成到商业化的有限元模拟软件平台中。利用二次开发后的有限元模拟软件平台模拟了该钛合金在热压缩过程中失稳变形区的分布及其变化。模拟预测结果与实验结果吻合较好, 说明所提出的失稳变形模拟与预测方法是可行和有效的。

**关键词:** 失稳图; 失稳变形; 失稳变形模拟; Ti–6.5Al–3.5Mo–1.5Zr–0.3Si; 钛合金

(Edited by Hua YANG)